Available online at www.sciencedirect.com
ScienceDirect
Journal of the European Ceramic Society 28 (2008) 1687–1696
www.elsevier.com/locate/jeurceramsoc

Microstructural features of the ZrO_2 interfacial coatings on SiC fibers before and after exposition to air at high temperatures

N.I. Baklanova [a,*], O.I. Kiselyova [b], A.T. Titov [c], T.M. Zima [a]

[a] *Institute of Solid State Chemistry and Mechanochemistry SB RAS, Kutateladze Street 18, Novosibirsk 630128, Russian Federation*
[b] *Lomonosov Moscow State University, Physical Department, Moscow, Russian Federation*
[c] *General Institute of Geology, Geophysics and Mineralogy SB RAS, Novosibirsk 630090, Russian Federation*

Received 30 October 2007; received in revised form 27 November 2007; accepted 30 November 2007
Available online 14 January 2008

Abstract

Sols of rare earth stabilized zirconia were used as simple, readily processable and accurate controllable precursors for the tetragonal zirconia interfacial coatings on commercially available SiC-based fibers. The tetragonal zirconia interfacial coatings can be applied to different types of SiC fibers without degrading fiber strength. The morphology, composition, structure, nanorelief and oxidation resistance of coated SiC fibers were evaluated by various analytical techniques, including scanning electron microscopy/energy dispersive analysis, transmission electron microscopy, atomic force microscopy in various modes, and micro-Raman spectroscopy. It was shown that the microstructural peculiarities of the $ReZrO_2$ interfacial coatings on SiC-based fibers may explain some of the differences in the behavior of different types of fibers.

Keywords: Interfacial coatings; Microstructure; ZrO_2; SiC fibers; Oxidation resistance

1. Introduction

Interface is a key region determining a set of properties of composite materials. In fiber-reinforced composites the fibers ensure the strength of material, while the matrix helps to keep the shape. The interface transfers the load from matrix to the fibers. Further, the incorporation of the reinforcing fibers into brittle ceramic matrix provides CMC's with a degree of pseudo-ductility, preventing catastrophic failure by several mechanisms, such as fiber debonding, fiber sliding and crack bridging.[1] In order to achieve these properties, the interphase zone must be sufficiently weak to deflect matrix microcracks and allow subsequent fiber pull-out. Both functions of the interphase zone in CMC's, namely, a load transfer from matrix to the fibers and the matrix microcrack deflection, are greatly determined by nature of the interphase zone. Despite of the wide recognition of the interphase as a crucial component of composites it remains one of the weakest links in the research of the matrix–interphase–fiber triad. Insufficient comprehension of interphase functions, role and nature, is a key problem and one major bottleneck retarding the development of efficient CMC's for high-temperature structural applications. To solve this problem it is necessary to study thoroughly the properties of interphase and to clarify which characteristics of the interphase and in what extent control the behavior of the composite. Undoubtedly, among the features of the interphase zone a microstructure is one of the most important.

In addition to above-mentioned functions (load transfer and crack deflection), interphase materials must be compatible with both matrix and fiber for long-term operation in oxidizing atmosphere. This is especially important for non-oxide CMC's, e.g. SiC/SiC composites. The interphase can be exposed to oxidizing environments when the ends of coated fibers are exposed to surrounding atmosphere or when matrix cracks are present, allowing oxidants to reach the fiber coatings. Since oxide ceramics cannot be oxidized, it is commonly believed that oxide-based coatings represent the best

* Corresponding author. Tel.: +7 3832 363839; fax: +7 3832 322847.
E-mail address: baklanova@solid.nsc.ru (N.I. Baklanova).

0955-2219/$ – see front matter © 2007 Elsevier Ltd. All rights reserved.
doi:10.1016/j.jeurceramsoc.2007.11.008

choice in terms of oxidation resistance. Several oxidation resistant and crack-deflecting materials including monazite, alumina/silica, stabilized zirconia, and others were proposed as appropriate candidates for interphase zone in CMC's.[2–8]

Some information is available in publications, describing the behavior of the stabilized ZrO_2-coated SiC fibers exposed to air at high temperatures.[9,10] Preliminary studying of the peculiarities of morphology and nanorelief of two zirconia-coated fibers, namely, Hi-Nicalon™ and Tyranno-SA™ before and after exposition to air at 1000 °C using atomic force microscopy (AFM) and scanning electron microscopy (SEM) showed that these features are greatly dependent on the type of SiC fibers. After application of coating the roughness of Tyranno-SA™ (nearly stoichiometric) fiber increased in comparison to that of the initial fiber, whereas the roughness parameters of Hi-Nicalon™ fiber retained their values after application of coating. Moreover, the difference in the roughness parameters for coated Tyranno-SA™ and Hi-Nicalon™ fibers was enhanced after exposition to air at 1000 °C.

The purpose of this work is to study the microstructural features of the $ReZrO_2$-coated SiC fibers type Hi-Nicalon™, Hi-Nicalon S™, and Tyranno-SA™ and the evolution of these features after exposition to air at 1000 and 1200 °C.

2. Experimental

2.1. Substrate and coating preparation

Hi-Nicalon™, Hi-Nicalon S™ (both Nippon Carbon Co. Ltd., Tokyo, Japan) and Tyranno-SA™ grade 3 (Ube Industry Ltd., Yamaguchi, Japan) fiber tows were used as substrate materials. Prior to coating, Hi-Nicalon™ and Hi-Nicalon S™ fiber tows were immersed in 50:50 acetone/ethanol mixture for 24 h for removing a sizing agent, dried at ambient temperature and then thermally treated in air at 450 °C. Tyranno-SA™ fiber tow was immersed in hot distilled water for desizing, dried at ambient temperature and heated in air at 500 °C.

A detailed description of the coating procedure is given in Ref. [6] but some parameters of sol were optimized. Sol–gel approach was used for the preparation of multi-component rare earth oxide stabilized zirconia ($ReZrO_2$) coatings on all types of SiC-based fibers. At least two rare earth components were incorporated in conventional zirconia–yttria oxide system. Total content of rare earth oxides was 3 mol%. The coating stage involved firstly the immersion of the ceramic fiber tow into sol, drying in air at ambient temperature, slow heating till 1000 °C in vacuum and heat-treatment for 2 h.

2.2. Oxidation tests

Thermal oxidation resistance of coated ceramic fibers was examined in laboratory air under static conditions at 1000 and 1200 °C. The samples were placed into preliminarily heated furnace (KO-14, Germany) and kept there during fixed time intervals. Then the samples were taken out, cooled in dessicator and weighted with accuracy ±0.1 mg. The total time of testing was 40 h.

2.3. Specimen characterization

Scanning electron microscope SEM LEO 1430VP, supplied by EDX (Oxford) spectrometer was used for studying of morphology and composition of the initial and coated fibers.

Micro-Raman spectra of the $ReZrO_2$-coated ceramic fibers before and after oxidation were recorded using a Triplemate, SPEX spectrometer equipped with CCD spectrometric detector and microscope attachment for back scattering geometry. The 488 nm radiation from an argon laser was used for spectral excitation.

The topography and surface roughness of fibers was examined by atomic force microscopy (SolverP47Bio, NT-MDT, Russia) and MultiMode NanoScope IIIa (Veeco, USA) using TappingMode™. Silicon cantilevers were used. Filaments were attached to metal discs using double-sided adhesive tape. Different areas of several filaments of each type fibers were selected randomly. A roughness and other statistical parameters of selected areas were obtained using tool "Statistics" and FemtoScan 001 software for AFM images. The AFM images were flattened before analysis using second-order surface subtraction. Parameters were calculated based on following definitions. Mean roughness (R_a) is the arithmetic average of the absolute values of the surface height deviations, Z_{ij}, measured from mean plane:

$$R_a = \frac{1}{N_x N_y} \sum_{i=1}^{N_x} \sum_{j=1}^{N_y} |z|$$

Mean height (R_{mean}) is the arithmetic average of the absolute values of the measured heights:

$$R_{mean} = \frac{1}{N_x N_y} \sum_{i=1}^{N_x} \sum_{j=1}^{N_y} Z_{ij}$$

Maximum height roughness (R_{max}) is the difference in height between the highest and lowest points:

$$R_{max} = Z_{max} - Z_{min}$$

During the scanning, phase shifts, i.e. changes in the phase contact angle of vibration with respect to the phase angle of freely oscillating cantilever, were recorded simultaneously with height images.

2.4. Tensile strength tests

Mechanical tensile tests of the coated fibers were conducted at room temperature using FM-4 (Hungary) testing machine. Single fibers extracted from a tow were fixed on paper frame using a hard resin. The gauge of 10 mm in length was used. The diameter of each filament was measured in the middle of length by laser interferometry and used for calculation of mechanical properties of filaments. Next, the lateral sides of support frame were cut by a heated wire and the load was applied at constant crosshead speed of 1.3 mm/min. About 50 filaments for each type of fibers were tested. The average diameters for the coated fibers were determined to be equal to

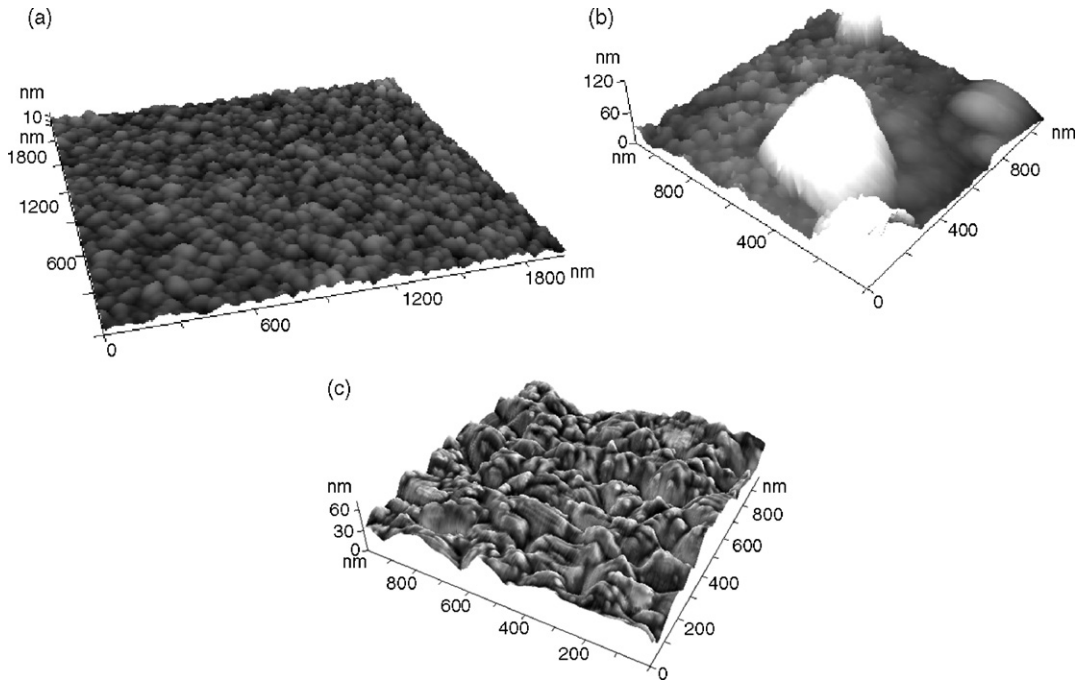

Fig. 1. The AFM images of the initial fibers (3D height representation): (a) Hi-Nicalon^{TM}; (b) Hi-Nicalon S^{TM}; (c) Tyranno-SA^{TM}.

13.94 ± 0.18 for Hi-Nicalon^{TM}, 13.11 ± 0.16 for Hi-Nicalon S^{TM}, and 7.53 ± 0.07 μm for Tyranno-SA^{TM} fibers.

3. Results

3.1. SEM/EDS, AFM and TEM analysis of as-received SiC fibers

AFM image of the initial Hi-Nicalon^{TM} fiber is represented in Fig. 1a. Filaments have very smooth and uniform surface. The estimated roughness parameter is about 5 nm and almost independent on the size of the scanned area. Contrary to Hi-Nicalon^{TM}, the surface relief of Hi-Nicalon S^{TM} filament is greatly non-uniform (Fig. 1b). Some areas have a rather homogeneous relief, while other areas consist of different size nodules. In some cases, their sizes run to several hundred nanometers. The disposition of nodules appears to be rather random and aperiodic. This picture is a typical one for all tested Hi-Nicalon S^{TM} filaments. There is a large scattering in the roughness parameters determined for different areas of the same filament. Roughness, R_a, was determined as 6–10 nm for scanned area of 4 μm^2. For areas with nodules the roughness is increased till about 25 nm. The difference in quality of the surfaces of both types of fibers probably to be related not only to the chemistry of the fiber but also to the other factors. Hi-Nicalon^{TM} is already successful within commercial market and thus the production parameters are strictly controlled for large quantities, whereas, Hi-Nicalon S^{TM} is a new monofilament with a limited production scale, and thus the parameters may still require further refinement in order to stabilize properties.[11]

AFM image of the initial Tyranno-SA^{TM} fiber is represented in Fig. 1c. It is clearly seen from these picture that this type fiber has very well-developed relief which can be due to large-size grains in the surface region of fiber, with lateral sizes of particles being 100–200 nm. Grains on the filament surface are disoriented. Phase contrast AFM images help to reveal minor features, which are sometimes poorly resolved, but only height images provide correct topographical data. When the surface relief contains elements, which vertical dimensions differ by the order of magnitude, it is difficult to demonstrate both types of elements in the same image. In order to increase the contrast in a 3D image, Fig. 1c was constructed by superposition of phase data over 3D topography. This type of representation shows minor details on 3D topographical relief. Roughness parameters, R_a and R_{mean}, were determined as 10 and 52 nm, respectively, for scanned area of 1.2 μm^2.

3.2. SEM/EDS, AFM analysis of the $ReZrO_2$-coated SiC fibers

SEM images of the $ReZrO_2$ (one dipping–annealing cycle) coating on Hi-Nicalon^{TM} fiber are represented in Fig. 2a–c. A distinctive feature of this coating is smoothness and uniformity along whole length and diameter of filaments. Separate well-developed crystals and discontinuity of the coating can be seen on the surface, but this is very rare occurrence. The thickness of coating determined by SEM is about 200 nm. From more close view of coated fibers one can see that the coating is formed by the radial oriented nanosized crystallites with a high aspect ratio. On separate filaments we observed dual orientation of the crystals, namely, parallel and perpendicular to filament axis (Fig. 2d). Earlier, it was shown that the orientation of crystals of the $ReZrO_2$ coating on Hi-Nicalon fiber is greatly effected by the properties of initial sol.[12] Close view of AFM (the height phase representation) and SEM images

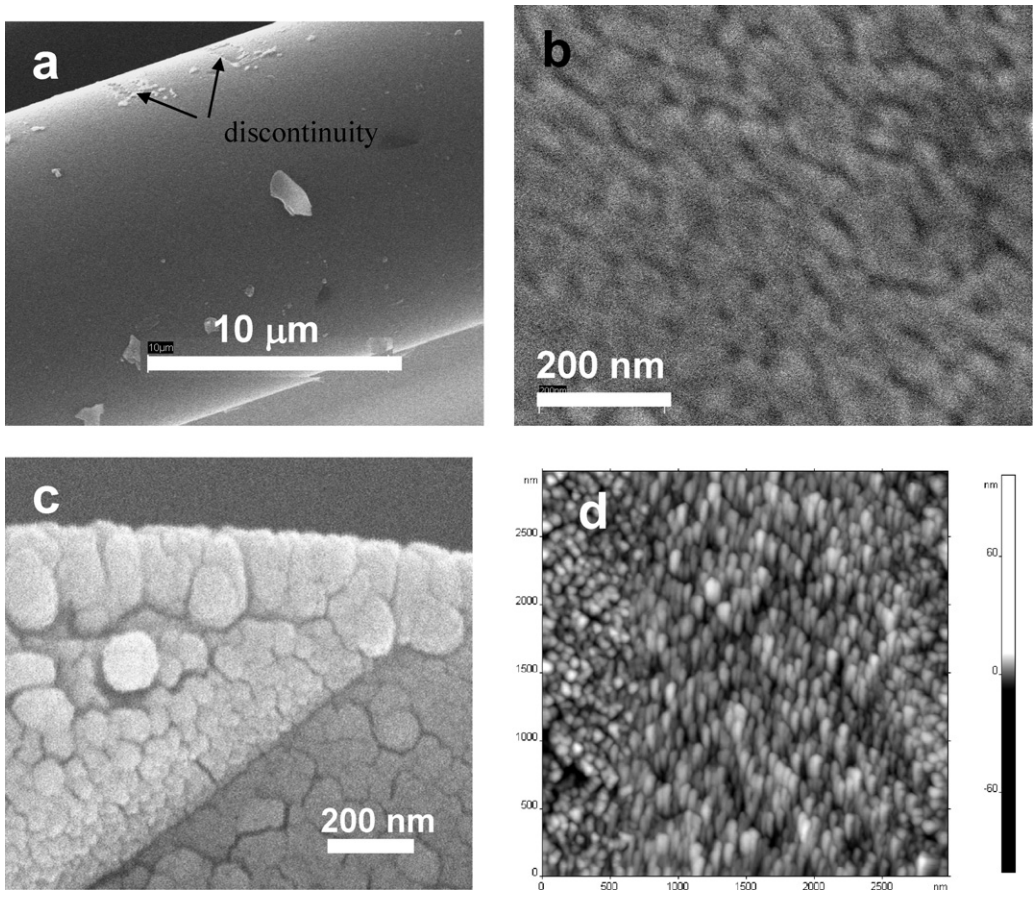

Fig. 2. The images of the surface and cross-section of the $ReZrO_2$-coated Hi-Nicalon^{TM} fiber: (a–c) SEM and (d) AFM (height representation).

suggests that the coating has nanosized porous structure (Fig. 2b and d).

No debonding of $ReZrO_2$ coating on Hi-Nicalon^{TM} fiber was observed. According to Patil and Subbarao[13], there is an anisotropy of thermal expansion for t-ZrO_2 along axis, the largest thermal expansion was determined to be along *a* and *c* axes (11.60×10^{-6} and $16.08 \times 10^{-6}\,^{\circ}C^{-1}$, respectively), the smallest along *b* axis ($1.35 \times 10^{-6}\,^{\circ}C^{-1}$). Thus, there is the large difference in CTE along two axes of t-ZrO_2 and Hi-Nicalon^{TM} fiber ($(3.5–4) \times 10^{-6}\,^{\circ}C^{-1}$). Based on this fact, one could expect that high thermal stresses during cooling of the coated fibers could cause debonding of coating. However, for all coated filaments under investigation no debonding was observed by high-resolution SEM analysis. Earlier, based on the X-ray spectroscopy studies of the Y-ZrO_2 coating on Nicalon^{TM} fiber, we found that the Zr–O–Si bonds were formed at the fiber–coating interface region of the Y-ZrO_2-coated Nicalon fiber.[6] White and coworkers[14] examined the ZrO_2/SiO_2 interfacial zone of thin ZrO_2 films on silicon using XPS and also presumed that the formation of the Zr–O–Si bonds takes place. Not only chemical bonding but also a dramatic rearrangement of the atomic coordinates exists at the ZrO_2/SiO_2 interface as was shown by Jarvis and Carter[15]. It appears to provide a significant source of interface strengthening even at ambient temperature and in the absence of a new reaction phase. Another reason for the absence of debonding under thermal stresses could be a porous structure of the coating (Fig. 2) that allows crystals of coating to expand.

Roughness parameters of the coated Hi-Nicalon^{TM} fiber were estimated after subtracting of second-order surface. Average roughness, R_a, and average amplitude, R_{mean}, were found to be 2.8 and 13.5 nm, respectively, over 3.5 μm × 3.5 μm area. They are practically independent on the scanned area size. This fact can be evidence in favor of very uniform relief of the obtained coating.

The morphology and topography of the $ReZrO_2$ coating on Hi-Nicalon S^{TM} fiber are somewhat distinct from those observed for Hi-Nicalon^{TM} fiber. Although the application of coating on Hi-Nicalon S^{TM} fiber gives rise to a smoothing of the surface relief of Hi-Nicalon S^{TM} ($R_a \sim 5$ nm for the coated fiber vs. $R_a \sim 7$ nm for the initial fiber for 4 μm^2 scanned area), separate large-size nodules were observed (Fig. 3a). They originate from as-received fiber. The coating is composed of crystals aligned perpendicularly to the surface of filaments and has porous structure. Again, no debonding of coating was observed.

Although the coating on Tyranno-SA^{TM} fiber is formed by rather coarse crystallites, it is uniform along length and diameter of filaments (Fig. 3b). The presence of zirconium was confirmed by EDX analysis taken from different parts of the coating (Fig. 3c). Non-uniformities such as large-size pores and crystals are practically absent for filament batch studied. AFM

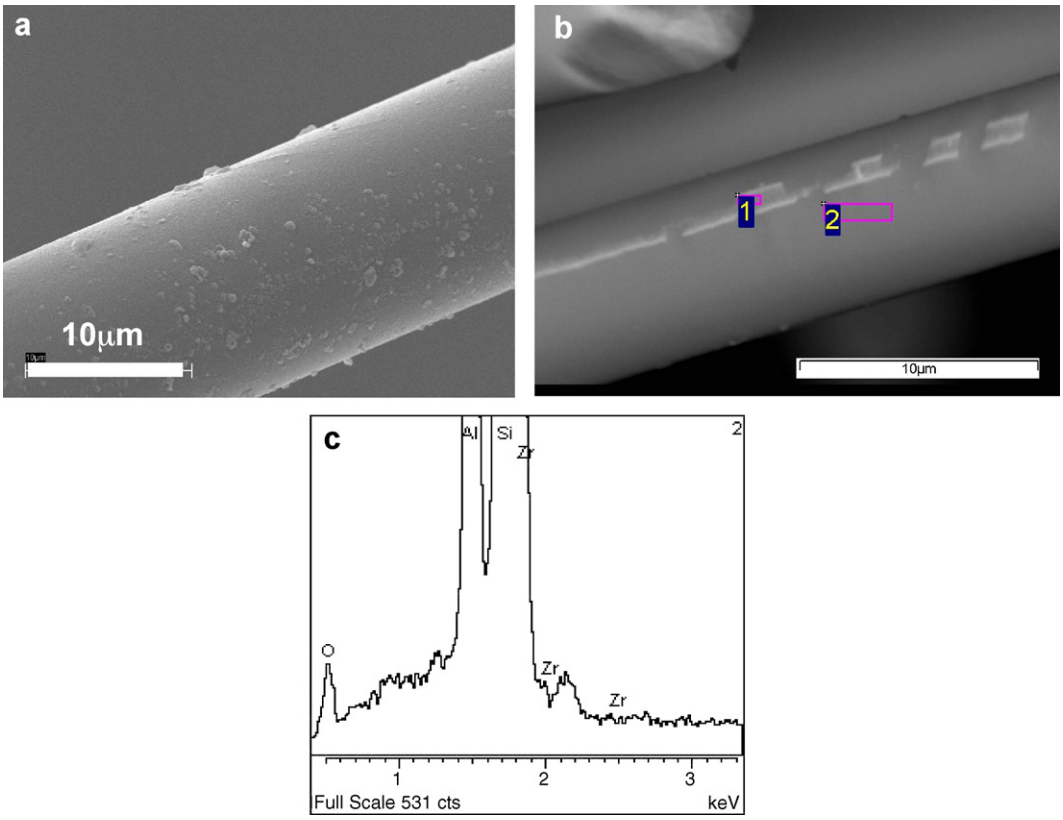

Fig. 3. The SEM/EDX analysis data of the $ReZrO_2$-coated fibers: (a) Hi-Nicalon S^{TM} and (b and c) Tyranno-SA^{TM}.

roughness parameters estimated for the coated Tyranno-SA^{TM} fiber confirm this observation. Actually, R_a value was found to be 10–12 nm for scanned area of 1.7 μm × 1.7 μm in size and only slightly higher than that for the initial Tyranno-SA^{TM} fiber. R_{mean} values are also slightly higher than those for the initial fiber (~85 nm vs. ~60 nm). A comparison of the AFM images in height and phase contrast modes taken for the same scanned area of the coated fiber allowed us to detect interesting peculiarity, namely, the appearance of nanosized bright spots at the boundaries of main crystal phase (Fig. 4a and b). It could be discreetly proposed that these bright spots are belonging to the harder and less viscoelastic phase than the main phase. The nature and reasons for appearance of this phase are not clear. In any case, this phenomenon deserves to be more carefully and precisely studied in the future.

Micro-Raman spectra taken from the coated Hi-Nicalon^{TM}, Hi-Nicalon S^{TM}, and Tyranno-SA^{TM} fibers showed no any additional features besides those belonging to fibers themselves. The $ReZrO_2$ coatings (one dipping–annealing cycle) on SiC fibers appeared to be too thin for Raman measurements.

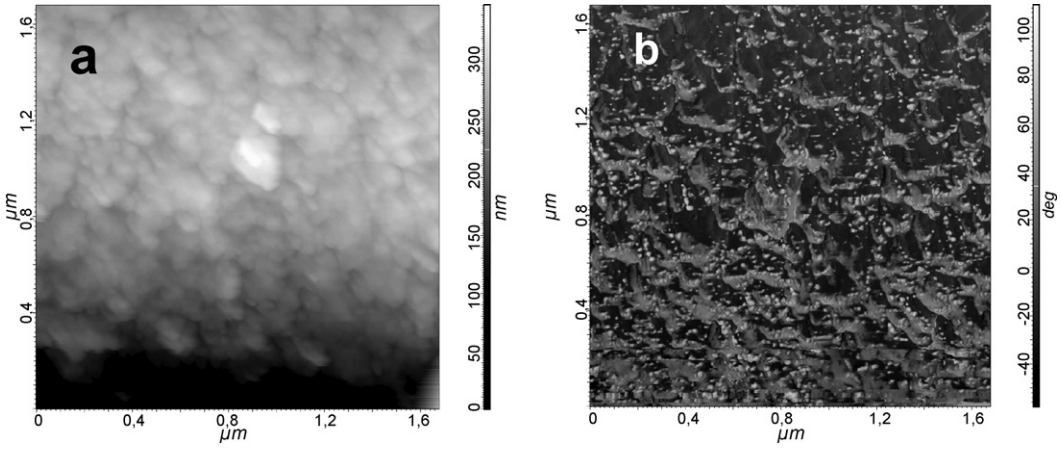

Fig. 4. The AFM images of the $ReZrO_2$-coated Tyranno-SA^{TM} fiber: height (a) and phase (b) representation of the same area of surface.

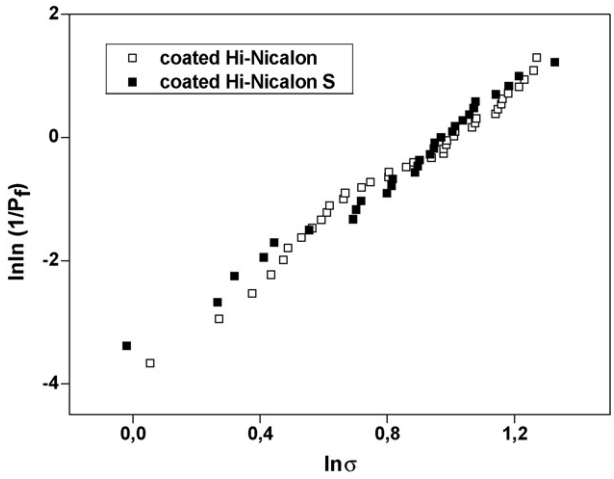

Fig. 5. Weibull probability plots for room temperature tensile strengths of the $ReZrO_2$-coated Hi-Nicalon^{TM} and Hi-Nicalon S^{TM} fibers.

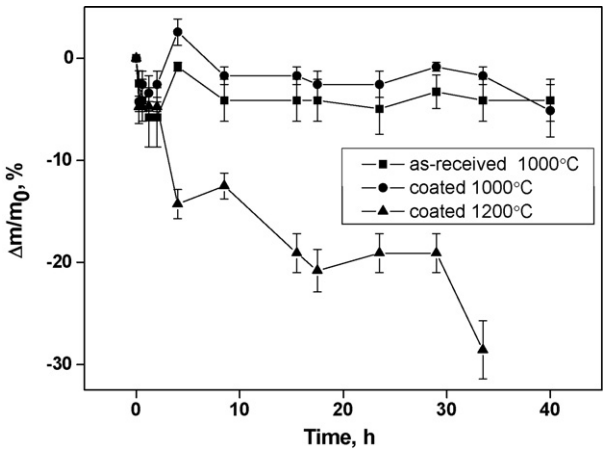

Fig. 6. Dependences of the relative mass $\Delta m/m_0$ on time for the initial and coated Tyranno-SA^{TM} fiber at 1000 and 1200 °C.

3.3. Tensile strength measurements

It is well known that mechanical properties of fiber-reinforced CMC's depend not only on the interfacial stress transfer capacity but also on mechanical properties of fibers.[1] Because of tensile strength fibers can be greatly influenced by coating, it is very important to determine the tensile properties of the coated SiC fibers in order to evaluate their ability as reinforcement for CMC's. In this study the single filament tensile tests of the $ReZrO_2$-coated fibers were performed at room temperature. The strength data for individual fibers were obtained using measured values of diameter of each filament, after that the data were analyzed using two-parameter single-modal Weibull function. The $\ln(1/P_f)$ vs. $\ln\sigma$ Weibull probability plots for $ReZrO_2$-coated Hi-Nicalon^{TM} and Hi-Nicalon S^{TM} fibers are represented in Fig. 5. The tensile strength and the Weibull modulus were found to be 2.71 ± 0.08 GPa and 3.73, respectively, for the $ReZrO_2$-coated Hi-Nicalon^{TM} fiber. The tensile strength is in good agreement with that reported in literature[14,16] for desized fiber. The tensile strength for the Hi-Nicalon S^{TM} fiber is 3.14 ± 0.10 GPa and this value is slightly higher that those for the initial desized fiber. The Weibull modulus was found to be 4.20. The increase in the fiber strength appears to be related to the elimination of the surface flaws by the $ReZrO_2$ coating. The most part of the $ReZrO_2$-coated Tyranno-SA^{TM} filaments were broken at the edge of frame during tensile strength measurements and data population was small in number. Therefore we could not extract the Weibull parameters from the obtained data.

3.4. The oxidized $ReZrO_2$-coated SiC fibers

Dependences of the relative mass $\Delta m/m_0$ on time for the as-received and $ReZrO_2$-coated Tyranno-SA fibers (one dipping–annealing cycle) at 1000 and 1200 °C are represented in Fig. 6. Both the as-received and coated fibers exhibit a similar behavior during oxidation test at 1000 °C, namely, (i) first a mass loss over a short period of time (~2 h); (ii) a slight mass gain; and (iii) gradual mass loss for long exposition. The mass loss of the initial and coated fibers at the beginning of oxidation is not more than several percents and could be attributed to burnoff of carbon. The following small mass gain could be due to oxidation of SiC that results in the formation of thin silica layer. The exposition of the coated fibers to air at 1200 °C leads to significant mass loss due to the volatilization of silicon- and carbon-containing compounds through the cracks and pores in the upper layer.[17]

SEM micrographs of the coated fibers after exposition to air at 1000 °C (40 h) are represented in Fig. 7a–c. As a whole, the coatings conserve their integrity, uniformity and smoothness. The round shape formations were observed on the surface of oxidized coated Hi-Nicalon S^{TM} fiber. They were present on the surface of coated fibers (Fig. 3a) and originated from the initial fiber (Fig. 1b). Contrary to Hi-Nicalon S^{TM}, the new formations

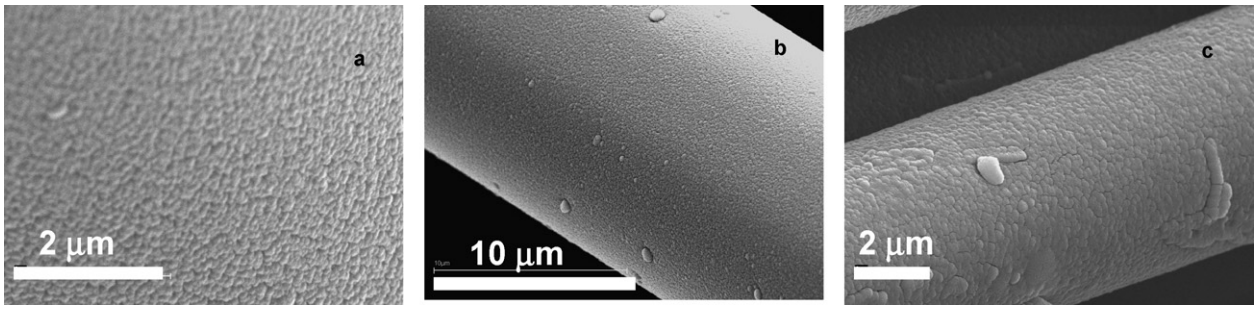

Fig. 7. SEM images of the $ReZrO_2$-coated Hi-Nicalon^{TM} (a), Hi-Nicalon S^{TM} (b) and Tyranno-SA^{TM} (c) fibers after exposition to air at 1000 °C for 40 h.

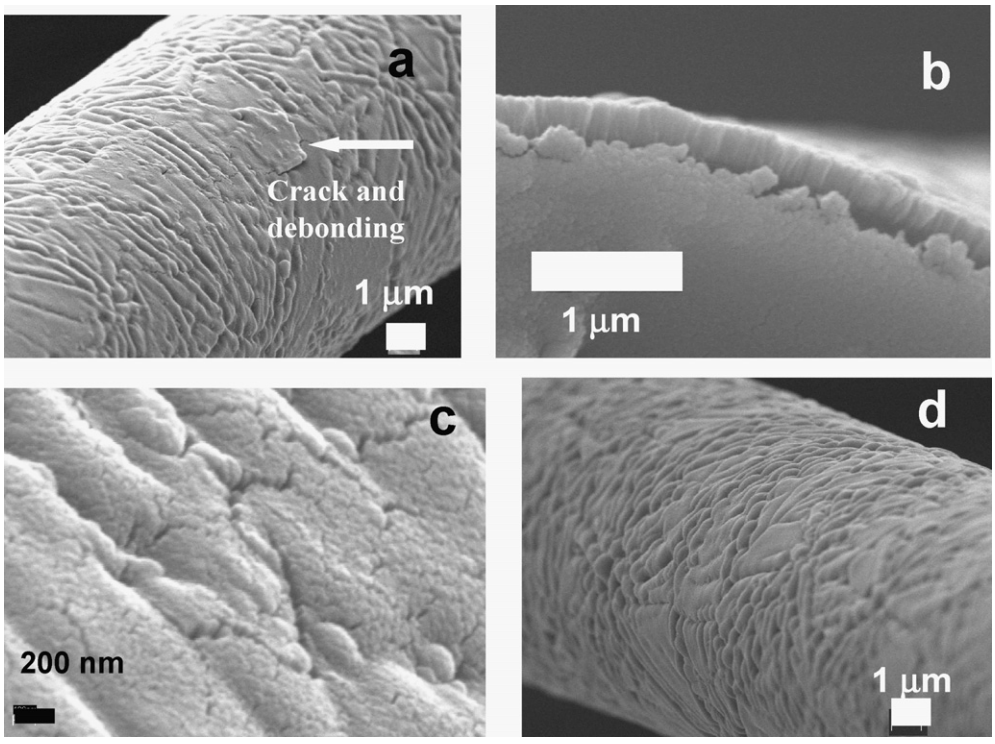

Fig. 8. SEM images of the initial Hi-Nicalon^{TM} (a–c) and Hi-Nicalon S^{TM} (d) fibers after exposition to air at 1200 °C for 40 h.

of large size which were observed on the surface of Tyranno-SA^{TM} fibers after exposition to air at 1000 °C (Fig. 7c). They are related to oxidation process. Indeed, the surface of the coated Tyranno-SA^{TM} fiber before high-temperature exposition to air was rather uniform according to SEM and AFM data and no any large-size grains were detected.

The surface relief of the initial fibers under investigation is drastically changed after exposition to laboratory air at 1200 °C (Fig. 8a–d). According to SEM analysis data, the surface relief of the initial Hi-Nicalon^{TM} fiber becomes rather rough and patterned. Nanosized pores are present between crystals. The thickness of oxidized upper layer was found to be ∼250 nm (Fig. 8b). In some cases, cracks and debonding of upper layer was observed (Fig. 8a and c). A similar patterned relief was observed for the oxidized initial Hi-Nicalon S^{TM} fiber (Fig. 8d). The surface of the oxidized initial Tyranno-SA^{TM} fiber was nodular.

SEM images of the surface of $ReZrO_2$-coated Hi-Nicalon^{TM}, Hi-Nicalon S^{TM} and Tyranno-SA^{TM} fibers after exposition to air at 1200 °C for 40 h are represented in Fig. 9a–c, respectively. The surface of oxidized coated fibers is not strongly distinguished from oxidized surface of the initial fibers and similar pattern relief was observed. No spalling of coating was detected and strong bonding between the fiber core and coating for all types of fiber is retained after long oxidation. The elemental microanalysis by SEM/EDS of oxidized coated fiber taken from different areas indicates the presence of Si, Zr, Al (as contamination from crucibles), and O. Although the $ReZrO_2$ coating has porous nanostructure and as a consequence, cannot protect fiber from oxidation in full extent, it has positive influence on oxidation behavior. As we observed (Fig. 8a and c), silica layer formed on the surface of uncoated fiber was cracked and debonded, hence, could not serve as effective barrier to oxygen, whereas $ReZrO_2$ coating was strongly bonded to SiC fiber.

Micro-Raman spectra taken from the smooth surfaces of the oxidized $ReZrO_2$-coated SiC fibers demonstrate only the presence of peaks belonging to fibers itself. The coatings appeared to be very thin for Raman measurements. Raman spectra taken

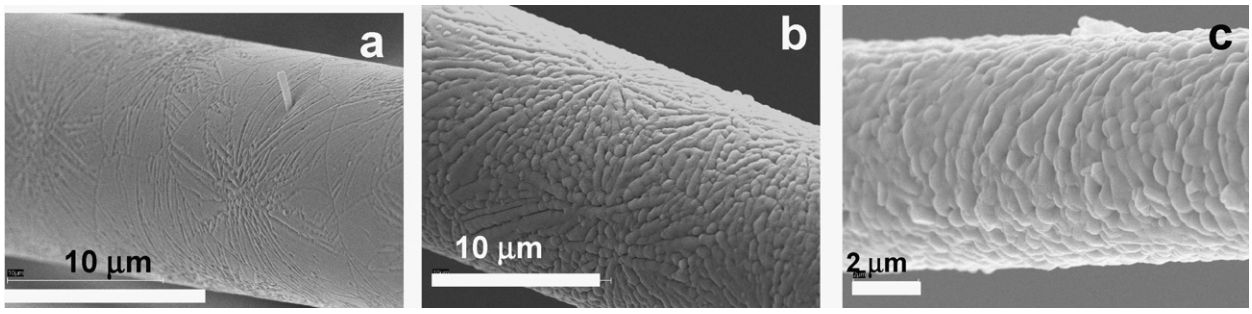

Fig. 9. SEM images of the $ReZrO_2$-coated Hi-Nicalon^{TM} (a), Hi-Nicalon S^{TM} (b) and Tyranno-SA^{TM} fibers (c) after exposition to air at 1200 °C for 40 h.

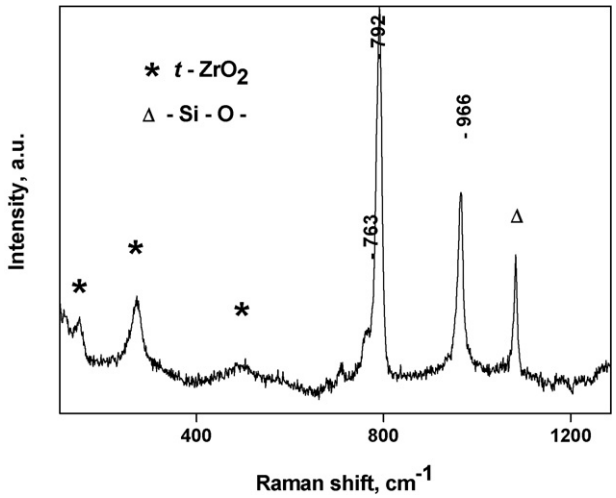

Fig. 10. Micro-Raman spectrum (λ = 488 nm) of the $ReZrO_2$-coated Tyranno-SA^{TM} fiber after exposition to air at 1200 °C for 40 h.

from large-size new formations on the surface of the oxidized $ReZrO_2$-coated Tyranno-SA^{TM} fibers clearly show the peaks belonging to t-ZrO_2 in the 100–700 cm^{-1} region (Fig. 10).[18,19] No peaks belonging to other ZrO_2 modifications were detected. Several peaks, which are in good agreement with those reported for Tyranno-SA grade 3 fiber[20] are also present in Raman spectrum. According to data,[20] peak (shoulder) at ∼760 cm^{-1} can be assigned to stretching of Si–C bonds in α-SiC, peaks centered at ∼792 and ∼966 cm^{-1} are belonging to stretching of Si–C bonds in β-SiC. Together with above-mentioned peaks, two main bands of amorphous carbon (so-called D and G bands) are also present in the 1200–1600 cm^{-1} region of Raman spectrum.

One can note that a new feature centered at ∼1084 cm^{-1} is observed in the spectrum of oxidized $ReZrO_2$-coated Tyranno-SA^{TM} fiber. The assignment of this feature is a question of special consideration. As this feature was observed only in Raman spectra of oxidized fibers it is reasonable to assume that it originates from the oxidation process and is related to either products of oxidation of SiC fiber itself (SiO_2 phases) or products of interaction of ZrO_2 with SiO_2 phases, namely, zircon. Indeed, according to literature data,[21,22] peak centered at about 1080 cm^{-1} is present in Raman spectra of SiO_2 phases (e.g. crystobalite and quartz), but its intensity is very low. The other peaks of these SiO_2 phases must be observed in the low frequency region (400–200 cm^{-1}). However, as was mentioned above, no any peaks other than belonging to t-ZrO_2 were detected in the 400–200 cm^{-1} region in Raman spectrum of oxidized coated fiber. It suggests that this feature cannot be related to stretching of the Si–O bond in SiO_2 phases. According to data by Syme et al.[23] and Lee and Condrate[24], peak at 1009 cm^{-1} is present in Raman spectrum of zircon ($ZrSiO_4$). This Raman shift does not coincide with that observed in this work. Hence, one can discreetly assume that phases other than SiO_2 and $ZrSiO_4$ are responsible for the appearance of this peak. One can note the affinity of the position of peak at 1080 cm^{-1} observable in Raman spectrum of the oxidized zirconia-coated Tyranno-SA^{TM} fiber to that reported for the asymmetric Si–O–Si stretching vibration that normally observed in spectra of organic silicon compounds.[21] This assignment seems to be reasonable taking into attention the fact that the composition of the as-received near stoichiometric SiC fiber is represented by mainly SiC phase together with very small quantity of graphite-like carbon. The long exposition of coated SiC fiber to air at high temperatures results in the oxidation of SiC and the formation of the Si–O–C structures.

4. Discussion

The same sol of the stabilized zirconia was applied to three types of SiC-based fibers. Hence, one could expect that some properties of the coated silicon carbide fibers will have a similarity. Actually, as one could see, the interfacial coatings are composed of tetragonal zirconia. The application of coatings resulted in a smoothing of the fiber relief. Coatings are continuous, well-ordered and rather uniform. The last is confirmed by AFM data on distribution of the measured heights and roughness parameters of the surface relief. The distribution of the measured heights of relief is the same or narrower compared with that for the initial fibers. The roughness parameters are lower compared with those for the initial fibers.

Based on these experimental results one can conclude that microstructure of the fiber is improved during the coating process. This conclusion has several important consequences in terms of the mechanical behavior of composite reinforced by the coated fibers. The first of them is a retaining or a slight increase of the filament tensile strength at room temperature due to the improved microstructure of the coated fibers. Actually, no any macrodefects which could be able to weaken a cross-section of fibers were detected on the surface of the coated fibers. Hence, one can expect that the overall strength of composite reinforced by stronger coated fibers will be also increased.

The other consequence is that a smooth relief of the coated fibers will provide easier sliding of the coated fibers relatively matrix and pull-out of fibers during the matrix crack propagation. Earlier, an extensive pull-out phenomenon for SiC/SiC composites reinforced by the $ReZrO_2$-coated Hi-Nicalon^{TM} and Hi-Nicalon S^{TM} fibers was observed by Baklanova and Lyakhov[25]. It was found that the fracture surface of the $ReZrO_2$-coated Hi-Nicalon^{TM} fiber composite was more fibrous in nature than that of Hi-Nicalon S^{TM} fiber composite and especially, compared with the composites reinforced by the uncoated fibers. The reason for this may be related to the smaller surface roughness of the $ReZrO_2$-coated Hi-Nicalon ^{TM} fiber compared with that for the uncoated fiber and $ReZrO_2$-coated Hi-Nicalon S^{TM} fiber. Fibers with high surface roughness have been found to have a pronounced influence on fiber sliding behavior in CMC's.[26–28]

The third consequence is in that the narrow distribution in sizes of particles of the coating provides a good stability of the coating microstructure during exposition at elevated temperatures. No significant grain growth was observed. This is especially true for Hi-Nicalon^{TM} fiber and in less extent for Tyranno-SA^{TM} and Hi-Nicalon S^{TM} fiber. As one can see, the roughness practically does not change for the coated

Hi-Nicalon^{TM} fiber and slightly increases for the coated Tyranno-SA^{TM} fiber even after exposition to air at 1000 °C.

Despite of the fact that all studied fibers are silicon carbide fibers and the same coating was applied to them, some of properties of interfacial coatings are greatly distinct from each other. Firstly, the coated Tyranno-SA^{TM} fiber surface is formed by more coarse crystallites than that of Hi-Nicalon^{TM} fiber. Besides, separate large crystallites are randomly disposed on the surface of the coated Tyranno-SA^{TM} fiber. Further, the interfacial roughness parameters for coated and uncoated Tyranno-SA^{TM} fiber are higher than those for Hi-Nicalon fiber^{TM}. The distribution of the measured heights of relief is wider than that for Hi-Nicalon^{TM} fiber attesting to a wider scatter in grain sizes. The difference in morphology of the coated fibers is enhanced after exposition to air at 1000 °C and especially at 1200 °C. The coated Tyranno-SA^{TM} fibers exhibit very intensive grain growth, with large grains growing due to small ones. It is sufficient to create critical flaws and to weaken the coated fibers.

Thus, one can conclude that microstructural peculiarities of the $ReZrO_2$ interfacial coating on SiC-based fibers, including morphology, porosity, nanorelief, the coating/fiber interface contribute to behavior of the coated fibers. Microstructure of the interphase may be as critical for thermostructural applications of CMC's, even if the service time of ceramic components will be relatively short.

5. Conclusion

Sols of rare earth stabilized zirconia were used as simple, readily processable and accurate controllable precursors for the ZrO_2 interfacial coatings on commercially available SiC-based fibers. The sol can be applied to different types of SiC fibers without degrading fiber strength. The morphology, composition, structure, nanorelief and oxidation resistance of coated fibers were evaluated by various analytical techniques, including SEM/EDS, AFM, and micro-Raman. It was shown that microstructural peculiarities of the $ReZrO_2$ interfacial coatings on SiC-based fibers may explain some of the differences in the behavior of different types of fibers.

Acknowledgements

The authors are grateful to Mrs. T.M. Naimushina for measurements of the tensile strength of filaments and Dr. B.A. Kolesov (Institute of Inorganic Chemistry SB RAS) for measurements of micro-Raman spectra.

References

1. Evans, A. G. and Marshall, D. B., Mechanical behavior of ceramic matrix composites. In *Fiber Reinforced Ceramic Composites*, ed. K. S. Mazdiyani. General Atomics, San Diego, CA, 1990, pp. 1–39.
2. Boakye, E. E., Mogilevsky, P., Parthasarathy, T. A., Hay, R. S., Welter, J. and Kerans, R. J., Monazite coatings on SiC fibers. I. Fiber strength and thermal stability. *J. Am. Ceram. Soc.*, 2006, **89**(11), 3309–3324.
3. Mogilevsky, P., Boakye, E. E., Hay, R. S., Welter, J. and Kerans, R. J., Monazite coatings on SiC fibers. II. Oxidation protection. *J. Am. Ceram. Soc.*, 2006, **89**(11), 3475–3480.
4. Verdenelli, M., Parola, S., Chassagneux, F., Letoffe, J.-M., Vincent, H., Scharff, J.-P. *et al.*, Sol–gel preparation and thermo-mechanical properties of porous xAl_2O_3–$ySiO_2$ coatings on SiC Hi-Nicalon fibres. *J. Eur. Ceram. Soc.*, 2003, **23**(8), 1207–1213.
5. Li, H., Lee, J., Libera, M. R., Lee, W. Y., Kebbede, A., Lance, M. J. *et al.*, Morphological evolution and weak interface development within chemical-vapor-deposited zirconia coating deposited on Hi-Nicalon^{TM} fiber. *J. Am. Ceram. Soc.*, 2002, **85**(6), 1561–1568.
6. Baklanova, N. I., Titov, A. T., Boronin, A. I. and Kosheev, S. V., The yttria-stabilized zirconia interfacial coating on Nicalon fiber. *J. Eur. Ceram. Soc.*, 2006, **26**(9), 1725–1736.
7. Meier, B., Grathwohl, G., Spallek, M. and Pannhorst, W., Sol–gel coatings on ceramic fibers for ceramic matrix composites. *J. Eur. Ceram. Soc.*, 1992, **10**(3), 237–243.
8. Colomban, Ph., Bruneton, E., Lagrange, J. L. and Mouchon, E., Sol–gel mullite matrix-SiC and mullite 2D woven fabric composites with or without zirconia containing interphase: elaboration and properties. *J. Eur. Ceram. Soc.*, 1996, **16**(2), 301–314.
9. Baklanova, N. I., Kolesov, B. A. and Zima, T. M., Raman study of yttria stabilized zirconium oxide interfacial coatings. *J. Eur. Ceram. Soc.*, 2007, **27**(1), 165–171.
10. Baklanova, N. I., Zaitsev, B. N. and Titov, A. T., Atomic force and scanning electron microscopy study of the zirconia-coated silicon carbon fibers. *J. Eur. Ceram. Soc.*, 2007, **27**(6), 2503–2511.
11. Morimoto, T. and Ogasawara, T., Potential strength of Nicalon, Hi Nicalon, and Hi Nicalon Type S monofilaments of variable diameters. *Composites: Part A*, 2006, **37**(3), 405–412.
12. Baklanova, N., Zima, T., Titov, A. and Zaitsev, B., Interfacial coatings on inorganic fibers for high temperature ceramic matrix composites. *Key Eng. Mater.*, 2008, in press.
13. Patil, R. N. and Subbarao, E. C., Axial thermal expansion of ZrO_2 and HfO_2 in the range room temperature to 1400 °C. *J. Appl. Cryst.*, 1969, **2**, 281–288.
14. Sun, Y. M., Lozano, J., Ho, H., Park, H. J., Veldman, S. and White, J. M., Interfacial silicon oxide formation during synthesis of ZrO_2 on Si(1 0 0). *Appl. Surf. Sci.*, 2000, **161**(2), 115–122.
15. Jarvis, E. A. A. and Carter, E. A., Exploiting covalency to enhance metal–oxide and oxide–oxide adhesion at heterogeneous interfaces. *J. Am. Ceram. Soc.*, 2003, **86**(3), 373–386.
16. Sha, J. J., Nozawa, T., Park, J. S., Katoh, Y. and Kohyama, A., Effect of heat treatment on the tensile strength and creep resistance of advanced SiC fibers. *J. Nucl. Mater.*, 2004, **329–333**, 5992–6602.
17. Zhu, Y. T., Taylor, S. T., Stout, M. G., Butt, D. P. and Lowe, T. C., Kinetics of thermal, passive oxidation of Nicalon fibers. *J. Am. Ceram. Soc.*, 1998, **81**(3), 655–660.
18. Lopez, E. F., Escribano, V. S., Panizza, M., Carnasciali, M. M. and Busca, G., Vibrational and electronic spectroscopic properties of zirconia powders. *J. Mater. Chem.*, 2001, **11**(7), 1891–1897.
19. Strekalovsky, V. N., Makurin, Yu. N. and Vovkotrub, E. G., Study of phase transformation and defects in the ZrO_2–Y_2O_3 system by Raman spectroscopy. *Inorg. Mater.*, 1983, **19**(6), 925–929 (in Russian).
20. Havel, M. and Colomban, Ph., Rayleigh and Raman images of the bulk/surface nanostructure of SiC based fibres. *Composites: Part B*, 2004, **35**(1), 139–147.
21. Socrates, G., *Infrared Characteristic Group Frequencies*. John Wiley and Sons, New York, 1980.
22. Nakamoto, K., *Infrared Spectra and Raman Spectra of Inorganic and Coordination Compounds*. John Wiley and Sons, New York, 1991, p. 120.
23. Syme, R. W. G., Lockwood, D. J. and Kerr, H. J., Raman spectrum of synthetic zircon ($ZrSiO_4$) and thorite ($ThSiO_4$). *J. Phys. C: Solid State Phys.*, 1977, **10**(6), 1335–1348.
24. Lee, S. W. and Condrate Sr, R. A., The infrared and Raman spectra of ZrO_2–SiO_2 glasses prepared by a sol–gel process. *J. Mater. Sci.*, 1988, **23**(11), 2951–2959.

25. Baklanova, N. I. and Lyakhov, N. Z., The development of components of advanced composite materials for structural applications. In *Proceedings of the IV International Technological Congress, Part 2*, ed. V. V. Shalay. OmSTU, Omsk, 2007, pp. 306–310.
26. Parthasarathy, T. A., Barlage, D. R., Jero, P. D. and Kerans, R. J., Effect of interfacial roughness parameters on the fiber pushout behavior of a model composite. *J. Am. Ceram. Soc.*, 1994, **77**(12), 3232–3236.
27. Jero, P. D., Kerans, R. J. and Parthasarathy, T. A., Effect of interfacial roughness on the frictional stress measured using pushout tests. *J. Am. Ceram. Soc.*, 1991, **74**(11), 2793–2801.
28. Brennan, J. J., Interfacial characterization of slurry-cast melt-infiltrated SiC/SiC ceramic matrix composites. *Acta Mater.*, 2000, **48**(18–19), 4610–4628.